ISTITUTO NAZIONALE DI FISICA NUCLEARE

Sezione di Milano

INFN/TC-95/20
14 Luglio 1995

D. Arginelli, C. Birattari, M. Bonardi, M. Gallorini, F. Groppi, S. Saponaro, L. Ulrici:

CALCULATION OF PRODUCTION RATES AND THICK-TARGET YIELDS FOR PLATINUM ISOTOPES PREPARED AT THE CYCLOTRON

PACS: 89.60

SIS-Pubblicazioni
dei Laboratori Nazionali di Frascati

INFN - Istituto Nazionale di Fisica Nucleare
Sezione di Milano

INFN/TC-95/20
14 Luglio 1995

CALCULATION OF PRODUCTION RATES AND THICK-TARGET YIELDS FOR PLATINUM ISOTOPES PREPARED AT THE CYCLOTRON

D. Arginelli, C. Birattari, M. Bonardi, M. Gallorini*, F. Groppi, S. Saponaro*, L. Ulrici
LASA, University and INFN–Sezione di Milano, Via F.lli Cervi 201, I–20090 Segrate Milano (Italy)

Abstract

The production of ^{191}Pt and ^{188}Pt by cyclotron irradiation can be carried out by direct reactions using α and proton beams on osmium and iridium targets respectively. The lack of data in the literature concerning the excitation functions for these nuclear reactions makes the optimization of the irradiation parameters impossible. This report includes a review of the few nuclear data available in the literature, some theoretical predictions about the beam energy necessary for the production of the two radioisotopes of interest and the results of some preliminary irradiations carried out with the variable energy cyclotron of JRC-Ispra (VA, Italy) of the EU at three different energies: 35 MeV for protons, 22 and 33 MeV for α particles.

streams of motorvehicles, makes it necessary to carry out toxicological studies on the possible effects of the emission of some trace metals, such as **platinum**, **palladium** and **rhodium**, on biological matrices [1,2,3]. The extremely low environmental concentration of these metals [4,5,6,7] requires a very sensitive analytical technique, such as the use of High Specific Activity Radiotracers (HSAR), to investigate their metabolic behaviour at low doses [8].

Among the Pt radioactive isotopes that can be produced by proton, deuteron or α beams, the most interesting from the half-life point of view [9,10] ($T_{1/2}$ comparable to the duration of the biological experiments envisaged) are reported in Table 1. Each production method shows different problems, related to the choice and preparation of the target, to the radiochemical separation adopted and to the spectral interferences among the radioisotopes produced. We will take into account only ^{nat}Ir(p,xn) and ^{nat}Os(α,xn) reactions; the ^{nat}Ir(d,xn) reactions are not considered because the production yield [11] for (d,xn) reactions is generally lower than that of the (p,xn). This depends mainly on two reasons: i) the maximum energy achievable in AVF cyclotrons for deuteron beams is the half of the corresponding value for protons, ii) deuteron stopping-power is greater than that of protons of the same energy. Furthermore, the Ir/Pt radiochemical separation shows relevant problems, due to the very low Ir chemical reactivity, whereas the Os/Pt radiochemical separation is more known and tested [12,13,14,15,16,17].

In Table 2, the main radioisotopes produced by side reactions, such as ^{nat}Ir(p,p xn) and ^{nat}Os(α,p xn) or ^{nat}Os(α,2p xn) with their Q-value, threshold energy (Th E), Incident particle Coulomb Barrier (ICB) and Outgoing particle Coulomb Barrier (OCB) are reported.

The state of the art concerning Pt radiotracers produced either by cyclotron or by reactor irradiation is not exhaustive. The results of the search carried out in the literature is reported in the references: some notes regard Pt isotopes employed in the biomedical field [3,13,18,19,20,21], others provide only some thick-target yield values (total beam energy absorption) for p or α particle irradiation [14,15].

In the cited literature, no data are reported about the thin-target excitation functions for Pt isotopes production by charged particles. For this reason, the optimized irradiation parameters (target thickness, beam energy, beam current intensity and irradiation time) can not be **exactly** predicted but can only be estimated by theoretical considerations (Th E, ICB) [22]. Moreover, some preliminary irradiations were necessary in order to select the most suitable energy to keep the production of radionuclidic interferents down.

Our interest was focused on ^{188}Pt and ^{191}Pt, because their characteristics are a good compromise among a $T_{1/2}$ suitable for medium term biochemical studies, reasonable γ-emission abundances, good γ-energies and few spectral interferences, as can be seen from Table 3. ^{189}Pt (721.5 keV, 5.5%), ^{193m}Pt (135.5 keV, 0.11%) and ^{195m}Pt (98.88 keV, 11.4%; 129.77 keV, 2.8%) have poor emission characteristics in both energy and abundance [9,10].

EXPERIMENTAL

The irradiations were carried out with the SCANDITRONIX MC40 cyclotron of the JRC-Ispra of the EU, whose maximum energy is 38 MeV for both proton and α beams. Iridium metallic foils (Ir > 99.9 %, Goodfellow Metals - UK) and some osmium powdered targets (Os LAB purity, Merck - FRG), pressed at 100 kg/cm^2 between two aluminium foils 16 μm thick, were used. Table 4 reports the target thickness, the beam and the energy used, the irradiation time and the integrated charge for the various experiments carried out.

Small aliquots of the chemically dissolved irradiated targets were analyzed by γ-spectrometry with HPGe detectors (EG&G Ortec - USA) accurately calibrated in both energy and efficiency using ^{226}Ra and ^{152}Eu certified γ-sources (Amersham, CEA). The radioisotopes decay was followed from 24 hours to 2 months from the End Of Bombardment (EOB) in order to detect the medium and long $T_{1/2}$ isotopes. For each γ-emission that seemed to be not contaminated, the corresponding radionuclide activity at the beginning of the γ-spectrum measurement $A(t_{BOM})$ versus time from the EOB was reported, where the expression

$$A(t_{BOM}) = \frac{C_\gamma}{\alpha_\gamma \, \varepsilon_\gamma \, \Delta t}\left(\frac{\lambda \, \Delta t}{1 - e^{-\lambda \Delta t}}\right) = \frac{C_\gamma}{\alpha_\gamma \, \varepsilon_\gamma \, \Delta t} D(\Delta t) \qquad (1)$$

was adopted for a simple decay, and the relation

$$A(t_{BOM}) = \frac{\lambda \dfrac{C_\gamma}{\alpha_\gamma \, \varepsilon_\gamma} + \dfrac{\lambda}{\lambda - \lambda_F} A_F^{EOB}\left[\left(1 - e^{-\lambda \Delta t}\right) - \dfrac{\lambda}{\lambda_F}\left(1 - e^{-\lambda_F \Delta t}\right)\right]}{1 - e^{-\lambda \Delta t}} \qquad (2)$$

was employed in the case of presence of a father radioisotope (F). In these relations λ ≡ radionuclide decay constant, α_γ ≡ γ-emission abundance, ε_γ ≡ equipment detection efficiency for the selected γ-emission, C_γ ≡ net experimental counts, Δt ≡ real counting time, D(Δt) ≡ decay factor during measurement, λ_F ≡ father decay constant and A_F^{EOB} ≡ father activity at the EOB. In both cases, $A(t_{BOM})$ is calculated considering the radioisotopes decay during the data acquisition. Whenever the curves obtained by eq. (1) and (2) did not turn out as the hypothetical ones, the γ-emissions per unit time ($C_\gamma / (\varepsilon_\gamma \, \Delta t)$) were employed for the graphs. The same replacement occurred if a theoretical interference was expected.

Fig. 1, 2, 3 and 4 show the decay curves for ^{188}Pt and ^{191}Pt (calculated using the underlined emissions in Table 3), that were fitted to obtain their activity at the EOB and to determine the production yield at the End of an Instantaneous Bombardment (Y_{EOIB}, i.e.: $\tau \rightarrow 0$) for ^{nat}Ir(p,xn)^{188}Pt, ^{nat}Ir(p,xn)^{191}Pt, ^{nat}Os(α,xn)^{188}Pt and ^{nat}Os(α,xn)^{191}Pt reactions. The relation applied to obtain these values is:

$$Y_{EOIB} = \frac{A_{EOB}\, G(\tau)}{Q} \qquad (3)$$

where $G(\tau) = \frac{\lambda\tau}{1 - e^{-\lambda\tau}}$ is the growing factor during the irradiation time τ and Q is the total beam charge collected. The choice of the γ-emission at 456.5 keV for the ^{191}Pt activity calculation depends on a higher detection sensitivity (taking into account the Compton background) with respect to the 172.2 keV emission, whose abundance value is however slightly superior [9,10].

Fig. 5 shows the 155 keV γ-emission of ^{188}Ir, produced by both direct reactions and ^{188}Pt decay; in this case, the Y_{EOIB} was not calculated. In order to determine the contribution to the production of ^{188}Ir by direct reactions and by ^{188}Pt decay, it was evaluated the experimental T^{ex}_{max}, that is the time of the maximum of the ^{188}Ir growing curve. If the contributes of the direct reactions were important, the T^{ex}_{max} would disagree with the theoretical value $T^{th}_{max} = (\ln\lambda - \ln\lambda_F)/(\lambda - \lambda_F) = 127.9$ h. Since the experimental T^{ex}_{max} = 129.5 h, we concluded that the direct (α,α xn) reactions are negligible under these irradiation conditions. The same conclusions can be obtained for the (p,xn) reactions.

Fig. 6 and 7 show the 539 keV γ-emission of ^{191}Pt produced via ^{nat}Ir(p,xn) and ^{nat}Os(α,xn) reactions; in both cases it is contaminated by $^{188}Pt \xrightarrow{\lambda_F} {}^{188}Ir \xrightarrow{\lambda} {}^{188}Os$. Since $\lambda_F < \lambda$, a transient equilibrium between the two isotopes is established; for this reason, after the $T^{th}_{max} = (\ln\lambda - \ln\lambda_F)/(\lambda - \lambda_F)$, the daughter ^{188}Ir appears to decay with the father's half-life. In order to determine the yield value for ^{191}Pt and to compare it with that obtained from Fig. 2, we carried out an exponential fit of the last experimental points of Fig. 6 (from $t_{EOB} > 11\ T^{191Pt}_{1/2} \approx 800$ h) due to ^{188}Pt and ^{188}Ir. The straight line obtained in the logarithmic scale was used to subtract the contribution of these two isotopes to the total γ-emissions per unit time for $t_{EOB} < 400$ h. The data obtained are related only to ^{191}Pt and, by another exponential regression, the EOB activity for this isotope can be calculated.

Radiochemical separation

As explained in the introduction, even if the yield obtained by ^{nat}Ir(p,xn) reactions is larger then that of the ^{nat}Os(α,xn) reactions, it was not possible to dissolve in any chemical medium the iridium targets (both metallic and powdered) at a reasonable rate. For this reason, the second production method was chosen.

Fig. 8 shows a simplified scheme of the Pt/Os radiochemical separation developed in order to obtain No Carrier Added ^{191,188}Pt. The powdered osmium target was dissolved in *aqua regia*, dried and then treated adding concentrated nitric acid. The osmium tetra-oxide was

distilled off by boiling, while the platinum containing residue was dried and redissolved in concentrated hydrochloric acid and then diluted with water. The platinum was reduced by Sn(II) to the divalent state and then purified from Sn(II) by extraction with ethyl ether from 3N HCl. Then the ether solution was dried and the residue redissolved in physiological solution. No other nuclides than platinum ones were detected in the final solution. The chemical separation yield was greater than 70%.

RESULTS AND DISCUSSION

Table 5 reports, for each target, the experimental thick-target yield for the Pt radiotracers of interest and some values of the radionuclidic interferents evidenced. The radionuclidic impurities not reported in this table were not detected due to either their too short half-lives and/or inadequate γ-emissions. The yield values of the (p,xn) reactions are much more larger than those of the (α,xn) for both ^{191}Pt and ^{188}Pt; moreover, the ratio between the two radioisotopes activity is different in the three cases: 2.1 for the Ir foil, 42.5 for TAR.1 and 15 for TAR.2. These different results can be explained considering that, apart from the different half-lives, ^{188}Pt is produced into the Os targets mainly by ^{186}Os(α,2n) reaction and ^{186}Os has a scarce isotopic abundance; on the contrary, ^{191}Pt is produced by (α,xn) or (p,xn) reactions induced on stable isotopes of Os and Ir respectively, that have a high isotopic abundance.

From Fig.1, 2, 3 and 4, it was calculated the experimental $T_{1/2}$ (related to the straight line slope) of the radioisotopes considered. Comparing these results with the corresponding listed values, we concluded that the selected γ-emissions for the yield values calculation were the best choice in our experimental conditions. Furthermore, the correlation coefficient for all the graphs is higher than 0.999.

The analysis carried out on Fig. 6 gives 840 MBq/C for the yield value for ^{191}Pt. Even if this result is different from the value of Table 5, it is acceptable considering that the analysis method used to determine it has a rough precision. On the contrary, in Fig. 7 the deviation from the straight line is not valuable and the resulting $T_{1/2}$ differs from the listed value for less than 0.3 %. Therefore, from the radionuclidic purity point of view, it seems more advantageous the production of ^{191}Pt based on the (α,xn) reaction method.

CONCLUSIONS

In order to investigate the metabolic behaviour of platinum, released in significant amounts from the automotive catalytic converters, the use of the High Specific Activity (HSA)

γ-emitting radiotracers ^{188}Pt and ^{191}Pt represents a very powerful tool. They both can be produced by cyclotron irradiation with proton and α beams and, in the latter case, can be radiochemically separated from the target to obtain No Carrier Added (NCA) tracers.

In this report it was described the production methods adopted in our laboratory in order to produce ^{191}Pt and ^{188}Pt. Two methods were investigated; each of them has different aspects to consider: the reactions induced by protons on Ir of natural isotopic composition show higher yield values with respect to the ^{nat}Os(α,xn) reactions for the tested energies; on the contrary, the Ir/Pt radiochemical separation was abandoned because of the extremely low dissolution rate of the target. The activity calculation should be carried out on different γ-emissions for each isotope, depending on the production method adopted. Concerning ^{191}Pt, we found that the 456 keV γ-emission was the best choice for the two considered methods even if, in the case of ^{nat}Os(α,xn) reactions, it could have been used also the emission of highest abundance (539 keV) for several days after the preparation of the tracer. As far as ^{188}Pt is concerned, all the γ–emissions present a theoretical interference; however, since the interferent ^{189}Pt has a short half-life with respect to ^{188}Pt, the 140.3 keV γ–emission was used for the yield calculation.

REFERENCES

(1) R.F.Hill, W.J.Mayer, Trans. Nucl. Sci., **24** (1977) 2549-2554.

(2) R.F.Hill, , N.M.Potter, Trans. Nucl. Sci., **26** (1979) 4704-4706.

(3) W.Moore, DHysell, L.Hall, K.Campbell, J.Stara, Env. Health Persp., **10** (1975) 63-71.

(4) V.Hodge, M.O.Stallard, Env. Sci. Techn., **20** (1986) 1058-1060.

(5) D.E.Johnson, J.B.Tillory, R.J.Prevost, Env. Health Persp., **12** (1975) 27-33.

(6) G.T.Vaughan, T.M.Florence, Sci. Total Env., **111** (1992) 47-58.

(7) M.Parent, R.Cornelis, F.Alt, K.Strijckmans, R.Dams, Biol. Trace El. Res., in press.

(8) E.Sabbioni, M.Bonardi, M.Gallorini, R.Pietra, S.Fontaner, G.P.Tartaglia, F.Groppi, J. Radioanal. Nucl. Chem., **160** (1992) 493-503.

(9) E.Browne, R.B.Firestone, Table of Radioactive Isotopes, ed. V.Shirley, John Wiley & Sons, 1986.

(10) U.Reus, W.Westmeier, Atomic and Nuclear Data Tables, Academic Press, New York, 1983.

(11) M.Bonardi, M.Silari, Phys. Med., **1** (1988) 23-46.

(12) J.D.Gile, W.M.Garrison, J.G.Hamilton, J. Chem. Phys., **19** (1951) 1426-1427.

(13) A.F.LeRoy, Env. Health Persp., **10** (1975) 78-83.

(14) M.Parent, K.Strijckmans, R.Cornelis, J.Dewaele, R.Dams, NIM B, **86** (1994) 355-366.

(15) H.L.Sharma, A.G.Smith, J. Radioanal. Chem., **64** (1981) 249-255.

(16) R.A.Nadkarni, G.H.Morrison, J. Radioanal. Chem., **38** (1977) 435-449.

(17) M.Parent, R.Cornelis, R.Dams, Anal. Chimica Acta, **281** (1993) 153-160.

(18) J.Baer, R.Harrison, C.A.McAuliffe, A.Zaki, H.L.Sharma, A.G.Smith, Int. J. Appl. Radiat. Isot., **36** (1985) 181-184.

(19) N.D.Tinker, A.Perera, H.L.Sharma, C.A.McAuliffe, Proc. VII Int. Symp. on Radiopharm. Chem., Groningen, (1988) 366-368.

(20) G.Toth, Int. J. Appl. Radiat. Isot., **31** (1979) 411-413.

(21) J.D.Hoeschele, T.A.Buttler, J.A.Roberts, C.E.Guyer, Radiochim. Acta, **31** (1982) 27-36.

(22) G.Friedlander, J.W.Kennedy, E.S.Macias, J.M.Miller, Nuclear and Radiochemistry, 3rd ed., Ed. John Wiley & Sons, New York (1981).

TABLE 1 - Pt radioisotopes produced via (p,xn), (d,xn) and (α,xn) nuclear reactions on ^{nat}Ir (^{191}Ir 37%, ^{193}Ir 63%) and ^{nat}Os (^{184}Os 0.02%, ^{186}Os 1.58%, ^{187}Os 1.6%, ^{188}Os 13.3%, ^{189}Os 16.1%, ^{190}Os 26.4%, ^{192}Os 41.0%) [9,10] with their Q-value, threshold energy (Th E) and Incident particle Coulomb Barrier (ICB), reported if lower than Th E.

Radioisotope	$T_{1/2}$	Production reactions	Q (MeV)	Th E (MeV)	ICB (MeV)
^{188}Pt	10.2 d	$^{191}Ir(p,4n)$	-23.9	24.0	-
		$^{191}Ir(d,5n)$	-26.1	26.4	-
		$^{186}Os(\alpha,2n)$	-18.9	19.3	21.3
		$^{187}Os(\alpha,3n)$	-25.2	25.7	-
		$^{188}Os(\alpha,4n)$	-33.2	33.9	-
^{189}Pt	10.89 h	$^{191}Ir(p,3n)$	-17.1	17.2	-
		$^{193}Ir(p,5n)$	-31.1	31.2	-
		$^{191}Ir(d,4n)$	-19.4	19.6	-
		$^{193}Ir(d,6n)$	-33.3	33.7	-
		$^{186}Os(\alpha,n)$	-12.1	12.4	21.3
		$^{188}Os(\alpha,3n)$	-26.4	27.0	-
^{191}Pt	2.9 d	$^{191}Ir(p,n)$	-1.8	1.8	11.4
		$^{193}Ir(p,3n)$	-15.8	15.8	-
		$^{191}Ir(d,2n)$	-19.6	19.8	-
		$^{193}Ir(d,4n)$	-21.4	21.6	-
		$^{188}Os(\alpha,n)$	-11.1	11.3	21.2
		$^{189}Os(\alpha,2n)$	-17.0	17.4	21.2
		$^{190}Os(\alpha,3n)$	-24.8	25.3	-
^{193m}Pt	4.33 d	$^{193}Ir(p,n)$	-1.0	1.0	11.4
		$^{193}Ir(d,2n)$	-3.1	3.1	11.0
		$^{190}Os(\alpha,n)$	-9.9	10.1	21.2
		$^{192}Os(\alpha,3n)$	-19.4	19.8	-
^{195m}Pt	4.02 d	$^{192}Os(\alpha,n)$	-5.1	5.2	21.1

TABLE 2 - Main radioisotopes produced by ^{nat}Ir(p, p xn) and ^{nat}Os(α, p xn) or ^{nat}Os(α, 2p xn) with their Q-value, threshold energy (Th E), Incident particle Coulomb Barrier (ICB reported if lower than Th E) and outgoing particle Coulomb Barrier (OCB).

Radioisotope	$T_{1/2}$	Production reactions	Q (MeV)	Th E (MeV)	ICB (MeV)	Th E +OCB (MeV)
^{187}Ir	10.5 h	^{191}Ir(p,p 4n)	-29.3	29.4	-	40.9
		^{184}Os(α,p)	-9.4	9.6	21.3	21.1
		^{186}Os(α,p 2n)	-24.3	24.8	-	36.3
		^{187}Os(α,p 3n)	-30.6	31.2	-	42.7
		^{188}Os(α,p 4n)	-38.5	39.4	-	50.9
^{188}Ir	1.73 d	^{191}Ir(p,p 3n)	-22.6	22.7	-	34.2
		^{186}Os(α,p n)	-17.6	18.0	21.3	29.5
		^{187}Os(α,p 2n)	-23.9	24.4	-	35.9
		^{188}Os(α,p 3n)	-31.9	32.5	-	44.0
		^{189}Os(α,p 4n)	-37.8	39.6	-	50.1
^{189}Ir	13.2 d	^{191}Ir(p,p 2n)	-14.4	14.5	-	25.9
		^{193}Ir(p,p 4n)	-28.4	28.5	-	40.0
		^{186}Os(α,p)	-9.4	9.6	21.3	21.1
		^{187}Os(α,p n)	-15.7	16.0	21.3	27.6
		^{188}Os(α,p 2n)	-23.7	24.2	-	35.7
		^{189}Os(α,p 3n)	-29.6	30.2	-	41.7
		^{190}Os(α,p 4n)	-37.4	38.2	-	49.7
^{190}Ir	11.8 d	^{191}Ir(p,p n)	-8.1	8.1	11.45	19.6
		^{193}Ir(p,p 3n)	-22.04	22.1	-	33.6
		^{187}Os(α,p)	-9.4	9.6	21.2	21.0
		^{188}Os(α,p n)	-17.36	17.7	21.2	29.2
		^{189}Os(α,p 2n)	-23.28	23.7	-	35.2
		^{190}Os(α,p 3n)	-31.08	31.7	-	43.2
$^{190m1}Ir$	1.2 h	^{191}Ir(p,p n)	-8.1	8.1	11.45	19.6
		^{193}Ir(p,p 3n)	-22.1	22.2	-	33.6
		^{187}Os(α,p)	-9.4	9.6	21.2	21.1
		^{188}Os(α,p n)	-17.4	17.7	21.2	29.2
		^{189}Os(α,p 2n)	-23.3	23.8	-	35.3
		^{190}Os(α,p 3n)	-31.1	31.8	-	43.2
$^{190m2}Ir$	3.2 h	^{191}Ir(p,p n)	-8.2	8.3	11.45	19.8
		^{193}Ir(p,p 3n)	-22.2	22.3	-	33.8
		^{187}Os(α,p)	-9.6	9.7	21.2	21.4
		^{188}Os(α,p n)	-17.5	17.9	21.2	29.6
		^{189}Os(α,p 2n)	-23.5	23.9	-	35.6
		^{190}Os(α,p 3n)	-31.2	31.9	-	43.3
^{191m}Ir	4.9 s	^{193}Ir(p,p 2n)	-14.1	14.2	-	25.7
		^{188}Os(α,p)	-9.4	9.6	21.2	21.1
		^{189}Os(α,p n)	-15.4	15.7	21.2	27.1
		^{190}Os(α,p 2n)	-23.2	23.7	-	35.0
		^{192}Os(α,p 4n)	-32.6	33.3	-	44.7

TABLE 2 - continued

^{192}Ir	74.02 d	$^{193}Ir(p,p\ n)$ $^{189}Os(\alpha,p)$ $^{190}Os(\alpha,p\ n)$ $^{192}Os(\alpha,p\ 3n)$	-7.7 -9.0 -16.8 -30.1	7.8 9.2 17.1 30.7	11.4 21.2 21.2 -	19.2 20.8 28.8 42.3
$^{192m1}Ir$	1.45 m	$^{193}Ir(p,p\ n)$ $^{189}Os(\alpha,p)$ $^{190}Os(\alpha,p\ n)$ $^{192}Os(\alpha,p\ 3n)$	-7.8 -9.1 -16.8 .26.3	7.8 9.2 17.2 26.9	11.4 21.2 21.1 -	19.3 20.9 28.6 38.3
$^{192m2}Ir$	241 y	$^{193}Ir(p,p\ n)$ $^{189}Os(\alpha,p)$ $^{190}Os(\alpha,p\ n)$ $^{192}Os(\alpha,p\ 3n)$	-7.9 -9.2 -16.9 -26.4	7.9 9.3 17.3 26.9	11.4 21.2 21.1 -	19.4 21.0 28.7 38.4
^{193m}Ir	11.6 d	$^{190}Os(\alpha,p)$ $^{192}Os(\alpha,p\ 2n)$	-9.1 -22.4	9.3 -22.9	21.1 -	20.7 34.5
^{194}Ir	19.15 h	$^{192}Os(\alpha,p\ n)$	-16.3	16.6	21.09	28.2
^{191}Os	15.4 d	$^{189}Os(\alpha,2p)$ $^{190}Os(\alpha,2p\ n)$	-14.7 -22.5	15.0 23.0	21.2 -	26.5 34.6
^{193}Os	1.27 d	$^{192}Os(\alpha,2p\ n)$	-22.7	23.2	-	34.8
^{194}Os	6.0 y	$^{192}Os(\alpha,2p)$	-15.6	15.9	21.09	27.5

TABLE 3 - Main γ-emissions (abundance >1%) for ^{188}Pt and ^{191}Pt radioisotopes and main theoretical interferences [10].

Radioisotope (decay)	γ-emission (keV)	Abundance (%)	Interferences
^{188}Pt	187.6	19.4	^{191}Pt (187.7 keV, 0.42%)
($^{188}Pt \xrightarrow{EC} {}^{188}Ir \xrightarrow{EC} {}^{188}Os$)	195.1	18.6	^{190}Ir (196.9 keV, 2.5%)
	381.4	7.47	^{190}Ir (380.0 keV, 1.96%)
	423.3	4.36	^{190}Ir (420.6 keV, 58.0%)
	140.3	2.33	^{189}Ir (141.1 keV, 2.62%)
	478.2	1.8	^{190}Ir (477.8 keV,1.8%)
^{191}Pt	538.9	13.7	^{191}Pt (538.1 keV, 0.24%)
($^{191}Pt \xrightarrow{EC} {}^{191}Ir$)	409.4	8.00	^{190}Ir (407.2 keV, 27.5%)
	359.9	6.00	^{190}Ir (361.1 keV, 12.6%)
	172.2	3.52	
	456.5	3.36	
	351.2	3.36	
	268.6	1.65	
	624.1	1.41	^{189}Pt (623.2 keV, 0.15%)

TABLE 4 - Irradiation parameters applied for the Pt isotopes production.

Target	Iridium metallic foil	Osmium pressed powder (TAR 1)	Osmium pressed powder (TAR 2)
Geometric characteristics	108 mg/cm^2 □ 7.5x7.5 mm^2	220 mg/cm^2 ∅ 12 mm	158 mg/cm^2 ∅ 10 mm
Beam particles	p	α	α
Beam energy on target	35 MeV	22 MeV	33 MeV
Beam mean energy loss into the target *	1 MeV	22 MeV	15.2 MeV
Time of irradiation	1 h	7 h	8 h **
Integrated charge	374 μC	7.7 10^4 μC	8.7 10^4 μC

*: Calculated with the TRIM code (J.F.Ziegler and J.P.Biersack).
**: Irradiation carried out in two steps, at 15 h 33 m one from the other.

TABLE 5 - Experimental production thin-target or thick-target yields for the interesting Pt radiotracers (calculated by the underlined γ-emissions of Table 3) and some values for the radionuclidic interferences obtained. The radionuclidic impurities not reported in this table were not detected because of their too short half-life or inadeguate γ-emissions.

	^{188}Pt yield	^{191}Pt yield	Radionuclidic interferences (production yield in kBq/(C MeV) or kBq/C), γ-emission utilized (abundance)
Iridium metallic foil	340 ± 2 MBq/(C MeV)	730 ± 12 MBq/(C MeV)	^{187}Pt (-) + ^{187}Ir (-), 913 keV (1.7%, 5.0%) ^{188}Ir (-), 155 keV (29.8%) ^{189}Pt (-), 721 keV (5.8%) ^{189}Ir ($1.27\ 10^5$), 276 keV (0.56%) ^{190}Ir ($7.3\ 10^4$), 519 keV (32.8%), 558 keV (29.0%) ^{192}Ir (-), 316 keV (82.9%) ^{193m}Pt (-), 135 keV (0.11%)
Osmium pressed powder (TAR. 1)	0.40 ± 0.01 MBq/C	17 ± 1 MBq/C	^{187}Pt (-) + ^{187}Ir (-), 913 keV (1.7%, 5.0%) ^{188}Ir (-), 155 keV (29.8%) ^{189}Pt (-), 721 keV (5.8%) ^{189}Ir (0.3), 276 keV (0.56%) ^{190}Ir (-), 519 keV (32.8%), 558 keV (29.0%) ^{192}Ir (-), 316 keV (82.9%) ^{193m}Pt (-), 135 keV (0.11%) ^{193}Os (-), 460 keV (3.95%) ^{194}Ir (-), 328 keV (13%) ^{195m}Pt (-) + ^{195m}Ir (-) + ^{195}Ir (-), 130 keV (2.83%, 1.7%, 1.4%)
Osmium pressed powder (TAR. 2)	16 ± 1 MBq/C	240 ± 3 MBq/C	^{187}Pt (-) + ^{187}Ir (-), 913 keV (1.7%, 5.0%) ^{188}Ir (-), 155 keV (29.8%) ^{189}Pt ($1.5\ 10^3$), 721 keV (5.8%) ^{189}Ir (18), 276 keV (0.56%) ^{190}Ir (0.25), 519 keV (32.8%), 558 keV (29.0%) ^{192}Ir (-), 316 keV (82.9%) ^{193m}Pt (130), 135 keV (0.11%) ^{193}Os (-), 460 keV (3.95%) ^{194}Ir (-), 328 keV (13%) ^{195m}Pt (-) + ^{195m}Ir (-) + ^{195}Ir (-), 130 keV (2.83%, 1.7%, 1.4%)

FIG. 1 - Decay curve for ^{188}Pt produced by $^{nat}Ir(p,xn)$ reactions. The error bars reported on the graph have statistical origin.

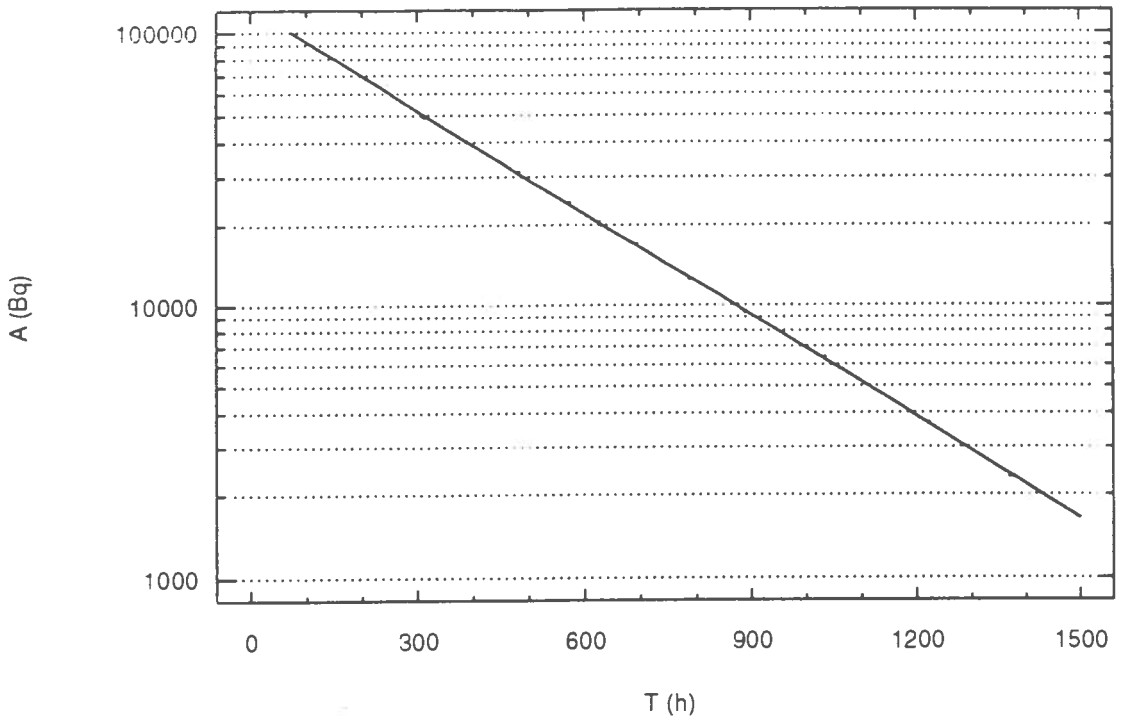

FIG. 2 - Decay curve for ^{191}Pt produced by $^{nat}Ir(p,xn)$ reactions. The error bars reported on the graph have statistical origin.

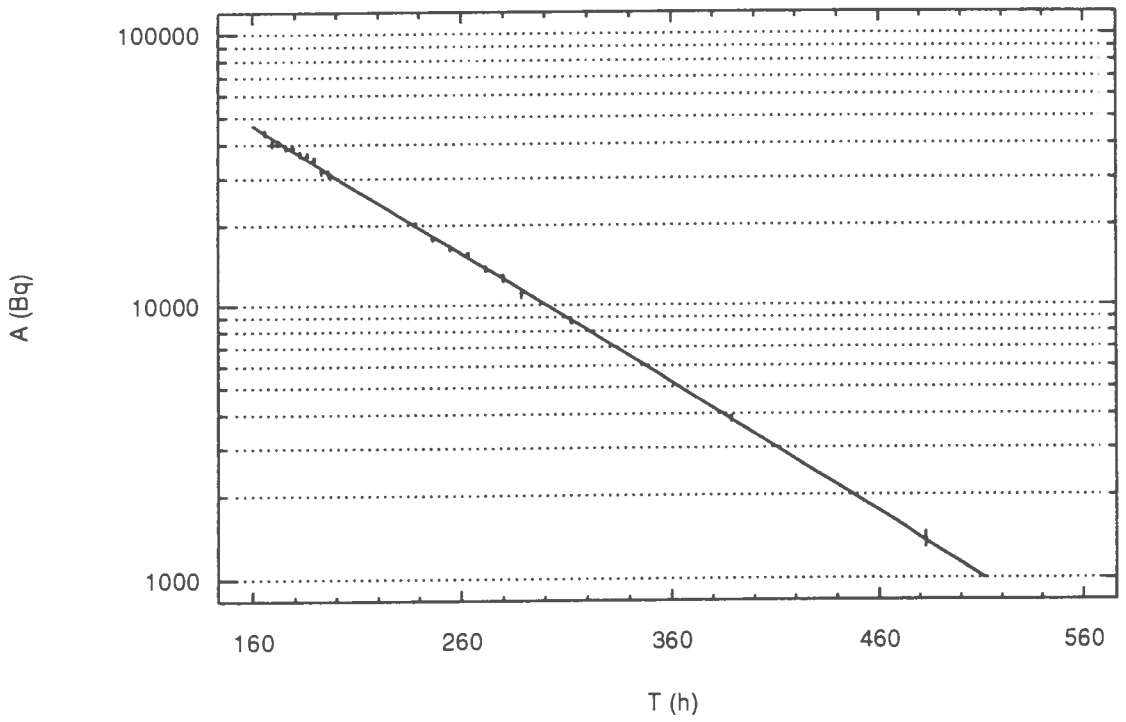

FIG. 3 - Decay curve for ^{188}Pt produced by $^{nat}Os(\alpha,xn)$ reactions. The error bars reported on the graph have statistical origin.

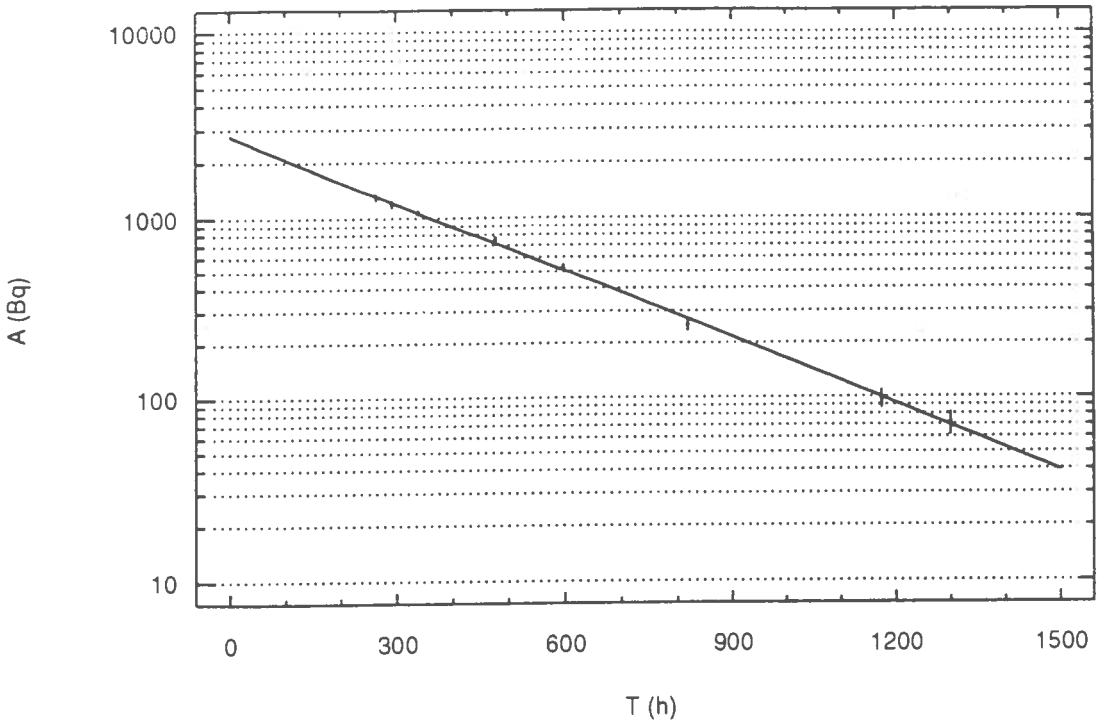

FIG. 4 - Decay curve for ^{191}Pt produced by $^{nat}Os(\alpha,xn)$ reactions. The error bars reported on the graph have statistical origin.

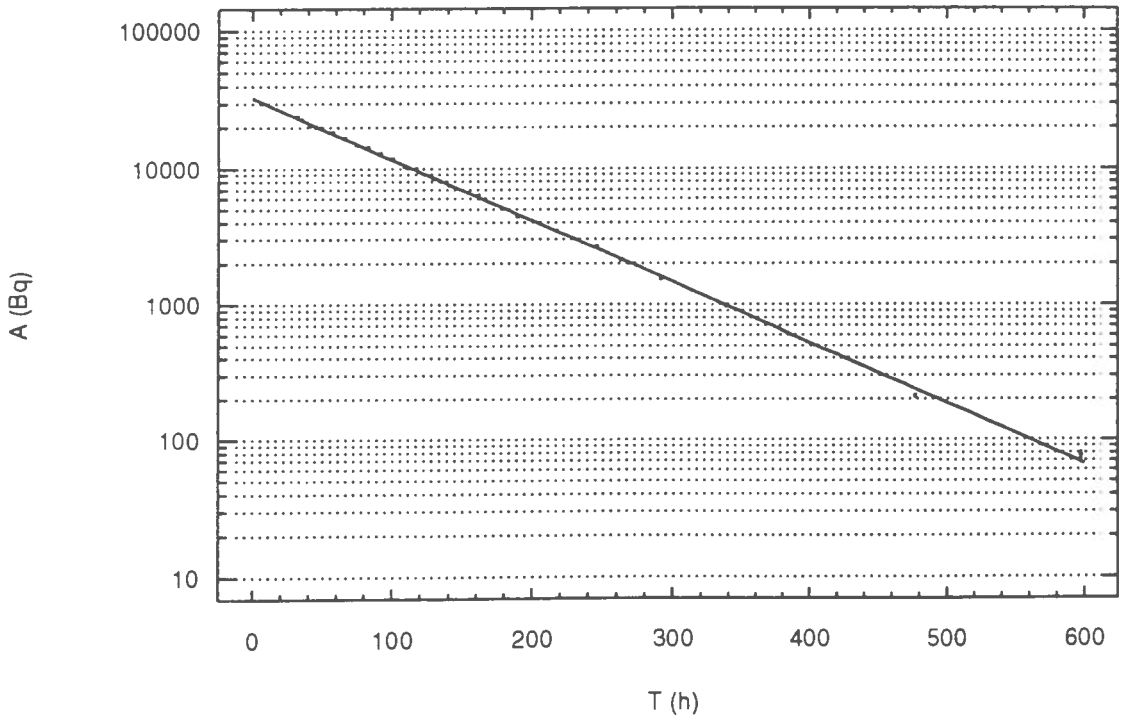

FIG. 5 - 155 keV γ-emission of ^{188}Ir, produced in TAR.2 by direct reactions and ^{188}Pt loading. The experimental T^{ex}_{max} and the theoretical $T^{th}_{max} = (\ln\lambda - \ln\lambda_F) / (\lambda - \lambda_F)$ are also reported.

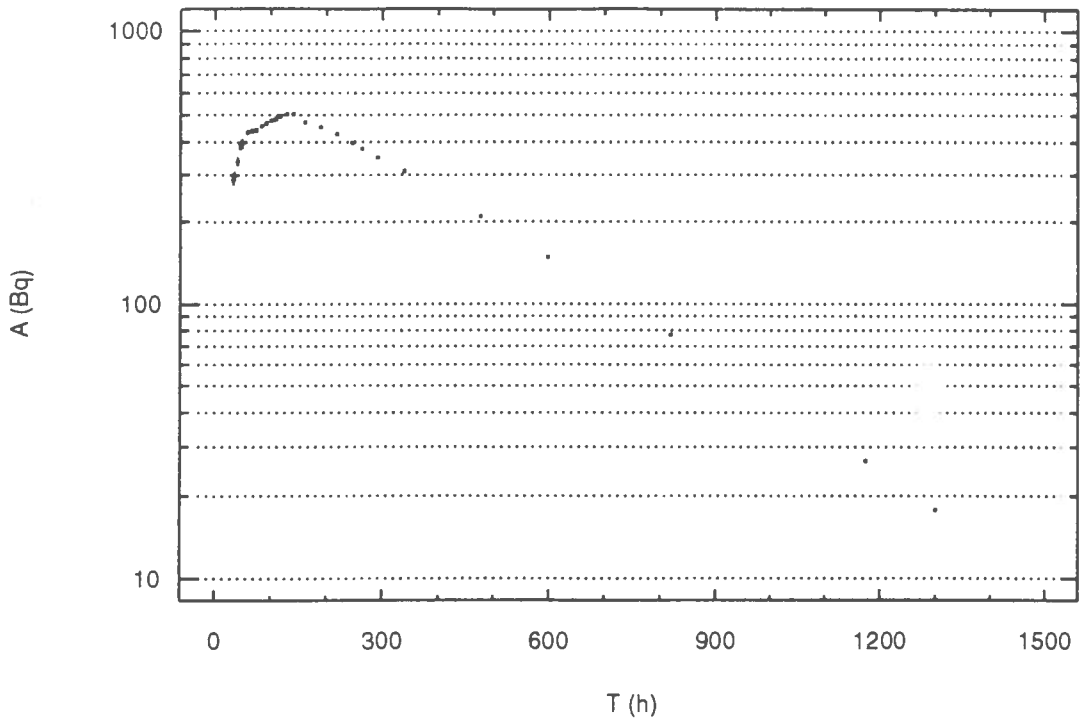

FIG. 6 - 539 keV γ-emission of ^{191}Pt produced via ^{nat}Ir(p,xn) reactions, contamined by ^{188}Pt.

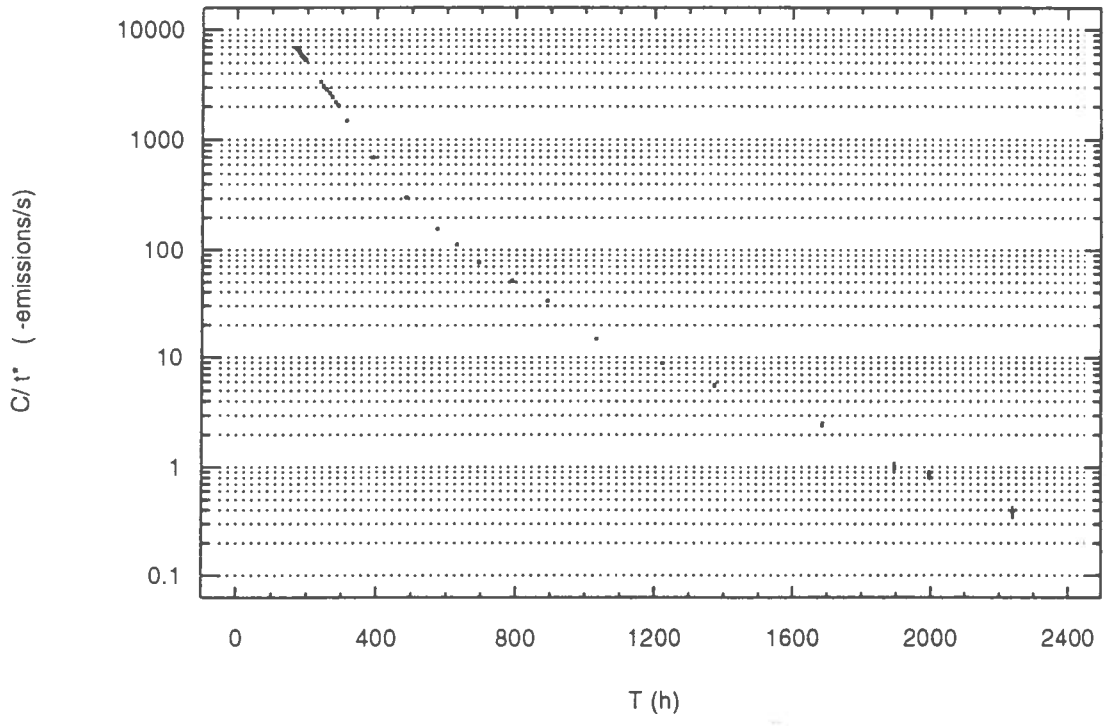

FIG. 7 - 539 keV γ-emission of ^{191}Pt produced via $^{nat}Os(\alpha,xn)$ reactions, contamined by ^{188}Pt.

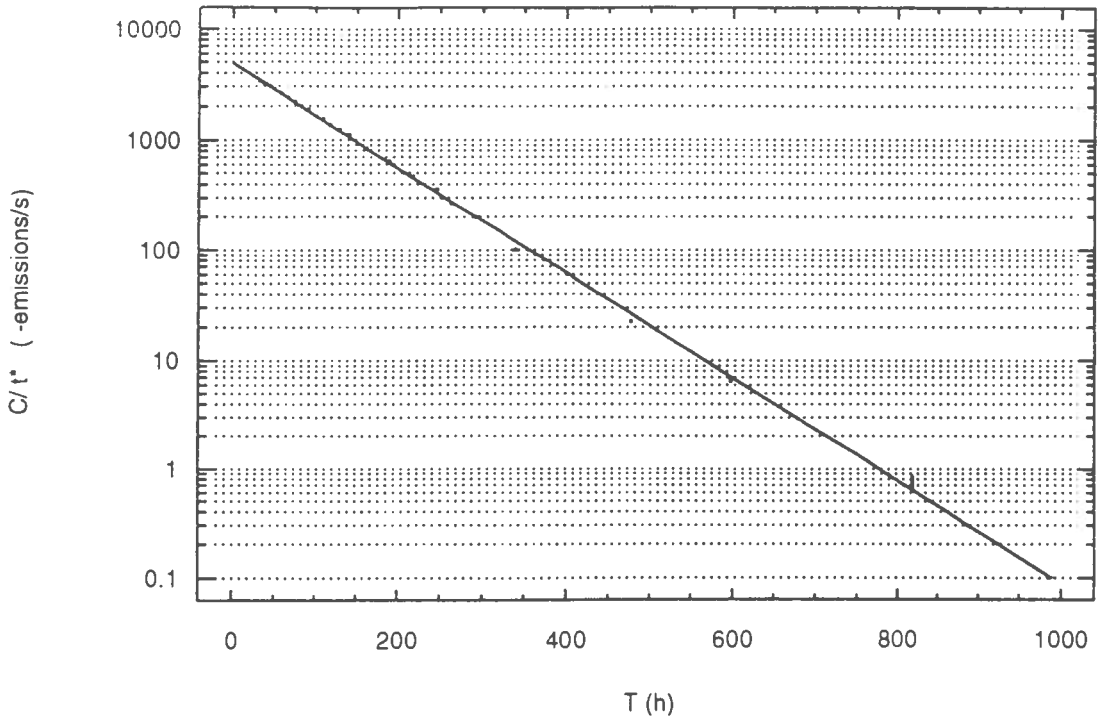

FIG. 8 - Simplified scheme of Os/Pt radiochemical separation.